Available online at www.sciencedirect.com

jmr&t Journal of Materials Research and Technology

https://www.journals.elsevier.com/journal-of-materials-research-and-technology

Original Article

Design of an esophageal deflection device for use during atrial ablation procedures

Karcher Morris[a,c], *Vlado A. Lubarda*[a,b,c,*], *Frank E. Talke*[a,c]

[a] *Department of Mechanical and Aerospace Engineering, UC San Diego, USA*
[b] *Department of NanoEngineering, UC San Diego, USA*
[c] *Center for Memory and Recording Research, UC San Diego, USA*

ARTICLE INFO

Article history:
Received 31 May 2020
Accepted 24 September 2020
Available online 8 October 2020

Keywords:
Cardiac ablation
Curved tube
Esophageal deflection device
Finite element analysis
Moment–curvature relation
Mooney–Rivlin model
Nonlinear elasticity

ABSTRACT

To prevent thermal damage of the esophagus during cardiac ablation surgery, a new device, named the esophageal deflection device (EDD), has been designed. The device consists of a curved elastic tube that is straightened by an inner rod (insertion rod) prior to insertion in the esophagus. After insertion of the assembled device in the esophagus, the insertion rod is pulled out, causing deflection of the esophagus as the tube returns to its original pre-curved shape. A nonlinear constitutive equation of the Mooney–Rivlin type was used to describe the mechanical response of the tube material (ethylene vinyl acetate), with material parameters determined experimentally through uniaxial tensile testing. An analytical expression based on nonlinear elasticity theory is derived for the relationship between moment and curvature and used to evaluate the moments required to straighten the initially curved tube. The force vs. deflection relation was determined experimentally in a setup designed to model the straightening of the pre-curved tube. A finite element model was also developed to evaluate displacements and stresses in both the pre-curved and the straightened tube, allowing qualitative comparison of analytical, numerical and experimental results.

1. Introduction

Atrial fibrillation (AF) is a common heart condition that affects tens of millions of people worldwide [1]. Cardiac electrophysiologists treat this disease with cardiac ablation, where a radiofrequency (RF) ablation catheter is inserted intravenously to thermally ablate the defective heart tissue. The esophagus lies directly behind the left atrium and is in close proximity to the heart during the ablation procedure. This close proximity of the esophagus poses a significant medical risk to the patient since it can lead to thermal injury of the esophagus [2,3]. To address the risk of thermal injury, surgeons currently use endoscopes, endotracheal stylets, or nitinol embedded rods to move the esophagus temporarily away from the heart [4–6]. These approaches pose additional risks to the esophagus, are time consuming, or require that an internist is on standby during the ablation surgery, which results in an increase of cost to the hospital.

In this paper, a new device, the so-called esophageal deflection device (EDD), is designed to protect the esophagus during ablation surgery by mechanically moving the esophagus away from the heart [7–9]. The EDD consists of two parts, a pre-curved flexible tube and an insertion rod. Prior to the procedure, the insertion rod is positioned inside the pre-curved tube, thereby straightening the tube for easy insertion. After

* *Corresponding author.*
https://doi.org/10.1016/j.jmrt.2020.09.123

the tube and insertion rod are inserted into the esophagus, the rod is pulled out and the tube reassumes its original pre-curved shape. During the process of reassuming its initial curvature, the tube applies a pressure to the esophageal wall and moves the esophagus away from the ablation site.

Medical devices have made use of pre-curved tubes in many applications, most notably in surgical robotics. Morimoto et al. [10], investigated experimentally the use of pre-curved concentric tubes for application in neurosurgery. Webster et al. [11] studied the mechanics of pre-curved tubes using Euler–Bernoulli beam theory and analyzed the deflection of multiple concentric tubes with various sizes and curvatures. Rucker et al. [12] implemented an analytical model for the geometry considered in [10] to account for large deformation of pre-curved tubes. Their analytical developments are founded from Antman's work [13] on Cosserat rod theory. Baek et al. [14] used finite element analysis to further study interaction of concentric tubes. Morimoto and Okamura [15] expanded the work of Webster et al. [11] by comparing beam mechanics theory to their experimental results measuring the curvature of initially pre-curved concentric tubes.

In the present work, we study thin polymeric tubes used in the Esophageal Deflection Device and investigate the effect of material and design parameters on the maximum stress and maximum force caused by the flattening of the pre-curved tubes. A nonlinear constitutive equation of the Mooney–Rivlin type was used for the tube material, with material parameters determined experimentally from uniaxial tensile tests. Pre-curved tubes were thermoformed and tested to evaluate the deformation of the tube with different curvatures and cross sections. A finite element simulation was developed to model the deformation of the tube, and its dependence on the materials properties. The analytical, experimental, and numerical results are discussed along with their applications to the final medical product.

2. Medical background

Atrial fibrillation (AF) is a common heart arrhythmia, or irregularity of the heart rate, which leads to a variety of health problems including chest pain, fatigue, or an increased likelihood of heart failure [1]. The mechanisms that cause AF are complex and are associated with irregularities of the electrical conduction system of the heart and atrial tissue characteristics [2]. Atrial ablation is a procedure that ablates defective heart tissue thermally. Ablation regions can be targeted by placing electrodes within the heart to perform, for example, pulmonary vein isolation that prevents irregular heart rate [2]. During the ablation procedure, esophageal tissue can be thermally damaged due to its proximity to the heart [3,16]. A rare and potentially fatal outcome of atrial ablation is the forming of an atrio-esophageal fistula, i.e., the creation of an opening between the heart and the esophagus due to the proximity and heat exchange between the left atrial wall and the esophagus [17,18]. It is common practice to utilize a temperature probe to measure luminal esophageal temperature during the ablation procedure. If the temperature rise is above a "safe" value, the cardiac electrophysiologist performing the surgery will stop the ablation procedure and move the esophagus away from the ablation region.

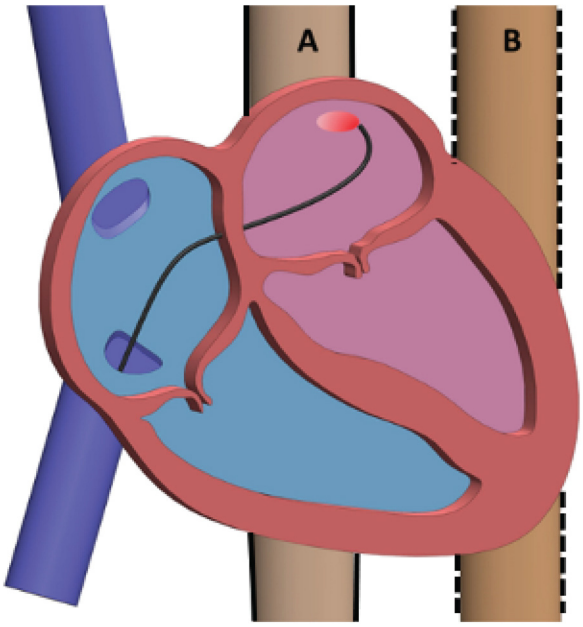

Fig. 1 – Schematic illustrating esophagus location A (undesirable) and location B (desirable) relative to the heart during a catheter ablation procedure.

A schematic of the heart and neighboring esophagus is shown in Fig. 1. Position A is the undeflected position of the esophagus, while position B is the deflected position of the esophagus, after moving it away from the ablation region. The esophagus is composed of two primary layers, a soft flexible muscular tissue and a more durable inner mucosa lining, with a thickness of approximately 3 mm for the muscle layer, and 2 mm for the mucosa layer [19]. The properties of human tissue and their variations within the esophagus and heart have been investigated [19,20]. These studies note the resilience of the esophageal tissue. Clinically used stents have also shown to expand radially and exert forces on the esophagus greater than 80 N when deployed at a diameter of 15 mm [21]. Moreover, Evonich et al. [22] showed, through experimental tensile tests of porcine tissue, that the structural integrity of esophageal tissue will remain intact even after thermal damage from ablation. To help in the analysis and understanding of this ablation procedure including thermal damage, finite element models have been designed to simulate the heat transfer from the ablation site to the esophagus [8,9,17,18]. Esophagus tissue has also been investigated using finite element analysis by taking into account the thick, foldable esophageal walls [23]. Furthermore, the relationship between an atrial retractor and the surrounding heart tissue has been examined by finite element simulations in [20].

3. Design of an esophageal deflection device (EDD)

Fig. 2 shows a 3D model of our esophageal deflection device originally proposed in [7,9]. The device consists of a pre-curved

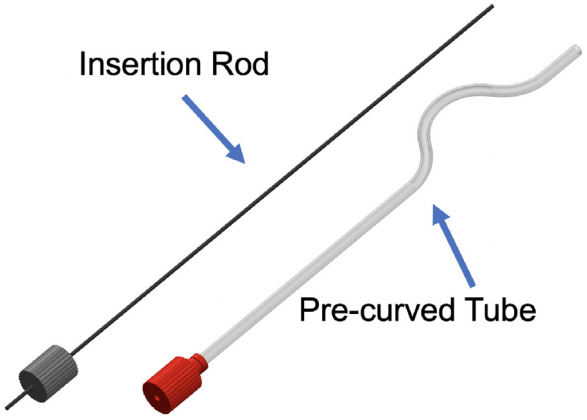

Fig. 2 – Computer aided design model of an esophageal deflection device (EDD) with tube and insertion rod.

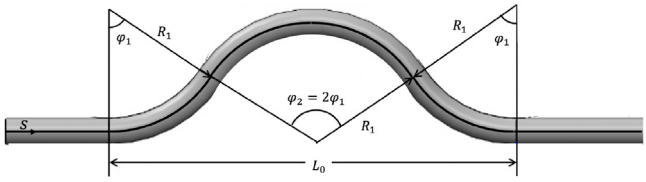

Fig. 3 – Schematic of pre-curved tube with geometric design parameters: the distance between the two ends of the curved portions of the tube is L_0, the radius of curvature is $R = R_1$ for all curved portions of the tube, and the corresponding angles are φ_1 and $\varphi_2 = 2\varphi_1$, so that $L_0 = 4R_1\varphi_1$.

flexible tube and an insertion rod. The pre-curved tube is straightened by the rod prior to its insertion in the esophagus. After insertion of the assembled device, the inner rod is pulled out, causing the deflection of the esophagus, as the tube tends to reassume its original curved shape. To manipulate the position of the esophagus during the surgery, the EDD may have to be inserted further, retracted, or twisted. After completion of the surgery, the EDD can be retrieved by slowly pulling on the handle of the assembled device. The inner rod may be fully inserted if more precise control of the esophagus position is desired by the surgeon during retrieval of the EDD.

To deflect the esophagus, important design parameters of the EDD are the tube's cross section (outer and inner diameter of the tube), the radius of curvature of the tube, and the bending stiff ness and strength properties of the material used. The assembled device including the tube and inner rod should be made "flexible enough" to navigate through the mouth and into the esophagus. We describe in this paper the idealized case of a rigid insertion rod to make our point clear. However, the inner rod must be "flexible enough" to cannulate the esophagus and does not need to be homogenous or uniform in its cross section. The design of the EDD must also take into consideration the mobility of the esophagus due to its interactions with adjacent soft tissue [21] and anatomical conditions including the diameter of the esophagus, the size of the heart, and the distance from the mouth. The tube should not exert pressure or forces on the inner esophageal wall that would exceed the limits tolerated by the human tissue. The quality and mechanical performance of the device should be tested further, beyond the force and deflection properties, to ensure patient safety. Tests for safe and reliable use should also be examined for anatomical variations of patients including children versus adults, and variability in tissue material properties. To satisfy FDA required ISO 10993 standards, the materials used in the EDD must be of biomedical grade and quality [24].

The assembled esophageal deflection device is inserted through the mouth into the esophagus. As the insertion rod is retracted, the tube reassumes almost fully its original curved shape (Fig. 3), depending on the position and stiffness of the surrounding tissue. In our EDD, the radius of curvature for all curved portions of the tube is $R = R_1$, and the distance between the two ends of the curved portions of the tube is L_0. The inner and outer radii of the hollow circular cross section of the tube are a and b, respectively. The change in the shape of the EDD tube from its initial curved position to the straight position by insertion of the stiff rod can be calculated by applying two pairs of opposite couples M and $2M$ at the cross sections corresponding to inflection points of the original curved shape of the tube. The magnitude of the couple M is chosen to eliminate the initial curvature of the tube ($\pm 1/R$). When the insertion rod is removed, the EDD goes back to its original shape and applies a pressure along the inner esophageal wall, thereby moving the esophagus away from the ablation site.

4. Constitutive equation for a rubber-like material

Correct constitutive equations are needed to model the EDD tube mechanical response during its deformation. If the tube material undergoes only small (infinitesimal) elastic strain, the stress σ is proportional to strain ϵ. For uniaxial stress, $\sigma = E\epsilon$, where E is the elastic modulus of the material. For the EDD tube under consideration, strains can be large and a nonlinear relationship between stress and strain must be considered to describe its mechanical response.

Hyperelastic material models of isotropic nonlinear elasticity are based on the elastic strain energy function $W = W(\lambda_1, \lambda_2, \lambda_3)$, where $\lambda_1, \lambda_2, \lambda_3$ are the principal stretch ratios (the eigenvalues of the stretch tensor $\mathbf{V} = \mathbf{B}^{1/2}$, where $\mathbf{B}$ is the right Cauchy–Green deformation tensor $\mathbf{B}$). For the Mooney–Rivlin isotropic and incompressible material model, the strain energy W is of the form [25,26]

$$W = C_1(I_B - 3) + C_2(II_B - 3), \tag{4.1}$$

where I_B and II_B are the invariants of $\mathbf{B}$, while C_1 and C_2 are the material parameters determined from experimental data. In the case of uniaxial stress, the stretch ratios in an incompressible isotropic material are $\lambda_1 = \lambda$, $\lambda_2 = \lambda_3 = 1/\sqrt{\lambda}$, where $\lambda = l/l_0$ is the ratio of the elongated and original length of the

specimen. The right Cauchy–Green deformation tensor **B** consequently becomes

$$\mathbf{B} = \begin{bmatrix} \lambda_1^2 & 0 & 0 \\ 0 & \lambda_2^2 & 0 \\ 0 & 0 & \lambda_3^2 \end{bmatrix} = \begin{bmatrix} \lambda^2 & 0 & 0 \\ 0 & 1/\lambda & 0 \\ 0 & 0 & 1/\lambda \end{bmatrix}, \tag{4.2}$$

with the corresponding invariants

$$\begin{aligned} I_B &= \lambda_1^2 + \lambda_2^2 + \lambda_3^2 = \lambda^2 + \frac{2}{\lambda}, \\ II_B &= \lambda_1^2\lambda_2^2 + \lambda_2^2\lambda_3^2 + \lambda_3^2\lambda_1^2 = 2\lambda + \frac{1}{\lambda^2}. \end{aligned} \tag{4.3}$$

The stress expression follows from the general expression for the Cauchy stress tensor $\boldsymbol{\sigma}$ of isotropic and incompressible hyperelasticity [25,26],

$$\boldsymbol{\sigma} = -p\mathbf{I} + 2\left(\frac{\partial W}{\partial I_B}\mathbf{B} - \frac{\partial W}{\partial II_B}\mathbf{B}^{-1}\right), \tag{4.4}$$

where the pressure p can be determined by solving the boundary-value problem under consideration; $\mathbf{I}$ is the identity tensor, and the exponent "−1" stands for the inverse. The substitution of (4.1)–(4.3) into (4.4) gives the expression for the applied longitudinal stress in a uniaxial tension,

$$\sigma = -p + 2\left(C_1\lambda^2 - \frac{C_2}{\lambda^2}\right). \tag{4.5}$$

Because the normal stress in the orthogonal direction is equal to zero under uniaxial tension, it also follows from (4.4) that

$$0 = -p + 2\left(\frac{C_1}{\lambda} - C_2\lambda\right) \quad \Rightarrow \quad p = 2\left(\frac{C_1}{\lambda} - C_2\lambda\right). \tag{4.6}$$

By substituting the expression for p from (4.6) into (4.5), the stress–stretch relationship is found to be

$$\sigma = 2C_1\left(\lambda^2 - \frac{1}{\lambda}\right) + 2C_2\left(\lambda - \frac{1}{\lambda^2}\right). \tag{4.7}$$

5. EDD tube material

Ethylene vinyl acetate (EVA) was chosen as a material for the EDD tube since EVA has been used previously in biomedical applications, is easily available, and has good mechanical properties. Table 1 lists materials properties of commercially available EVA-tubes [Hudson Extrusions, Inc].

The stress–strain relationship for the specific rubber-like, EVA co-polymer is not fully defined in Table 1, but is needed for evaluating the mechanical features of the EDD. In order to identify a constitutive model that properly describes its stress–strain relationship, uniaxial tensile tests were performed by creating EVA specimens from flattened tube cutouts, and testing them uniaxially (Fig. 4), while adhering to ASTM D-412 standards [27].

Fig. 5 shows the stress vs. stretch ratio for up to 15% tensile strain $\epsilon = \Delta l/l_0$ for five uniaxial specimens, where l_0 is the initial length of the specimen, l is its current length, and $\Delta l = l - l_0$ is the length change. The maximum stretch ratio considered was $\lambda_{max} = l/l_0 = 1.15$, which corresponds to maximum strain in the tube of length $L = 84$ mm and initial radius of curvature $R_0 = 27$ mm when it is straightened out by two end couples, as discussed in the next section. The material response is initially linear, but becomes increasingly nonlinear as the strain increases. To analytically describe this behavior, we adopted the Mooney–Rivlin constitutive model and determined the material parameters C_1 and C_2 by requiring that (a) the constitutive expression must reproduce the experimentally observed initial elastic modulus $E = 52.8$ MPa (slope of the stress–strain curve at zero strain), and (b) the applied stress at strain $\epsilon = 0.15$ is $\sigma = 3.71$ MPa, as experimentally observed. Thus, we required that

$$6(C_1 + C_2) = 52.8\,\text{MPa}, \quad 2C_1\left(1.15^2 - \frac{1}{1.15}\right)$$

Table 1 – Material properties provided by supplier.

Property	Nominal value unit	Test method
Melt mass-flow rate (MFR) (190 °C/2.16 kg)	2.3 g/10 min	ASTM D 1238
Vinyl acetate content	18.0 wt%	
Density	0.941 g/cm^3	ASTM D 1505
Durometer hardness (Shore D)	37	DIN 5305
Tensile strength at yield	4.5 MPa	ASTM D 638
Tensile strength at break	25 MPa	ASTM D 638
Ultimate elongation	820%	ASTM D 638
Vicat softening temperature	62 °C	ASTM D 1525

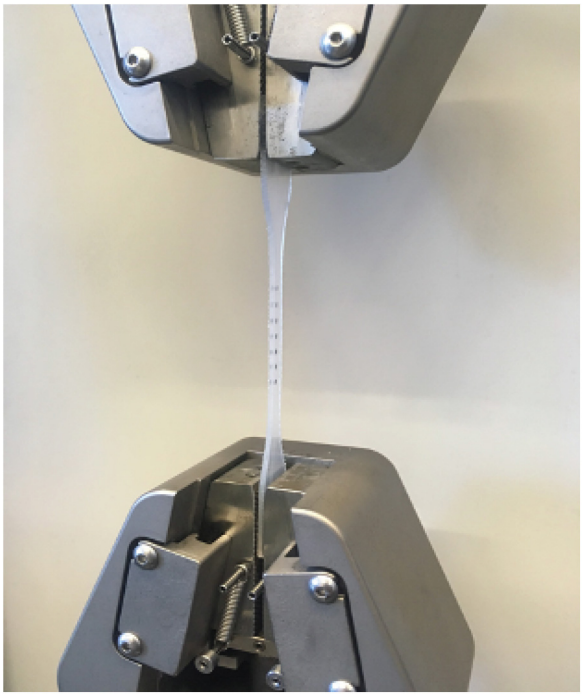

Fig. 4 – Uniaxial tensile testing of ethylene vinyl acetate tube material [MTS-Criterion tester]. The initial length of the specimen is $l_0 = 140$ mm, and the initial dimensions of the rectangular cross section are 3 mm × 1.59 mm.

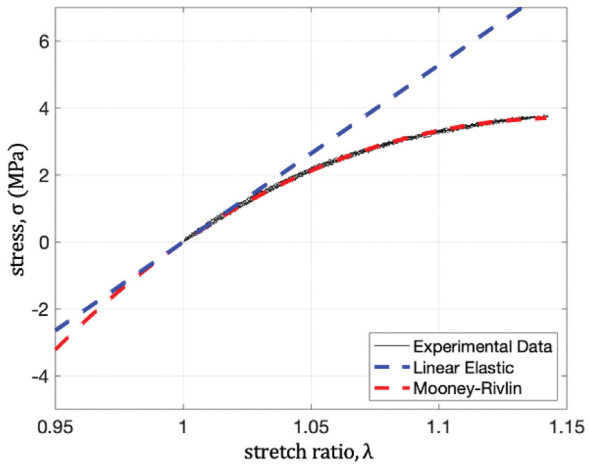

Fig. 5 – Experimental results for linear and Mooney–Rivlin models from EVA uniaxial tensile tests in the range of stretch ratio $0.95 \leq \lambda \leq 1.15$.

$$+2C_2\left(1.15-\frac{1}{1.15^2}\right)=3.71\,\text{MPa}. \tag{5.1}$$

This gives

$$C_1=-27.4\,\text{MPa},\quad C_2=36.2\,\text{MPa}. \tag{5.2}$$

We note that these values of the parameters C_1 and C_2 are intended to be used only for $0.95 \leq \lambda \leq 1.15$. For very large values of the stretch ratio λ, other values of C_1 and C_2 will be needed, but these large values of the stretch ratio are not of interest in the present work.

6. Moment–curvature relationship

Consider a pure bending of a slender circularly curved tube whose length along the centroids of the cross sections is L_0. The initial radius of curvature of the centroidal axis is R_0, such that $R_0\varphi_0 = L_0$, where φ_0 is the angle spanned by two end cross section of the tube (Fig. 6b). Each cross section is a hollow cylindrical cross section, made by two concentric circles of inner and outer radii a and b, respectively. Upon application of two end bending moments M in the vertical plane of symmetry, the tube bends and a longitudinal section in the vertical plane of symmetry becomes circular with the radius of curvature R of the longitudinal neutral axis of the tube, such that $R\varphi = L_0$. The neutral axis of each cross section is defined by the condition that $\sigma = 0$ along this axis. We adopt a simplified curved beam analysis in which we consider the normal stress orthogonal to the cross section of the beam only. If we locate the coordinate origin of the cross section at the point in the middle of the neutral axis, then the strain at a distance y from the neutral axis can be expressed as

$$\epsilon(y)=y\Delta\kappa,\quad \Delta\kappa=\frac{1}{R_0}-\frac{1}{R}, \tag{6.1}$$

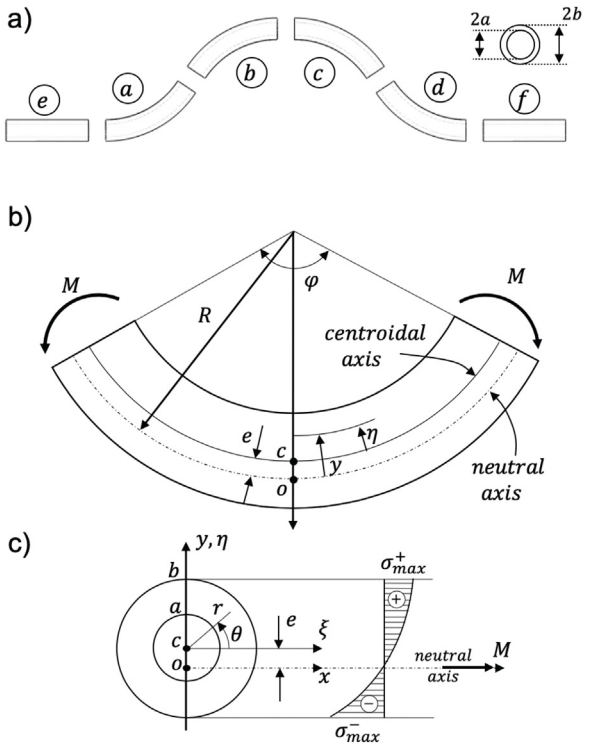

Fig. 6 – a) The EDD separated into four equivalent sections (a), (b), (c) and (d), and the straight sections (e) and (f) at the beginning and the end of the tube. (b) Generalized tube configuration with applied end moments M, the radius of curvature R, and other geometric parameters utilized in the analysis. (c) Cross section of the curved tube with the stress distribution along the vertical axis. The axis ξ passes through the centroid C of the cross section, while the neutral axis x passes through the point O at the distance e below the centroidal ξ axis.

where $\Delta\kappa$ is the change in curvature. Because the stretch ratio λ is related to strain ϵ by

$$\lambda=1+\epsilon=1+y\Delta\kappa, \tag{6.2}$$

the substitution of (6.2) into (4.7) gives

$$\sigma=2C_1\left[(1+y\Delta\kappa)^2-\frac{1}{1+y\Delta\kappa}\right]+2C_2\left[1+y\Delta\kappa-\frac{1}{(1+y\Delta\kappa)^2}\right]. \tag{6.3}$$

Under pure bending, the net normal force in each cross section of the tube must vanish, and the moment of the normal stresses $\sigma=\sigma(y)$ for any point must be equal to M, i.e.,

$$N=\int_A \sigma\,dA=0,\quad M=\int_A \eta\sigma\,dA, \tag{6.4}$$

where the centroid of the cross section is conveniently used as the reference point for the moment calculation. The vertical

distances from the centroid of the cross section (η) and from the neutral axis (y) are related by

$$y = \eta + e \tag{6.5}$$

with e being the vertical distance between the axes x and ξ, as shown in Fig. 6c. Upon the substitution of (6.5) into the first expression in (6.4), we obtain

$$C_1\left[\int_A (1+y\Delta\kappa)^2 dA - \int_A \frac{dA}{1+y\Delta\kappa}\right] + C_2\left[\int_A (1+y\Delta\kappa)\,dA - \int_A \frac{dA}{(1+y\Delta\kappa)^2}\right] = 0. \tag{6.6}$$

Because (ξ, η) are the centroidal axes of the cross section, it follows that

$$\int_A \eta\, dA = 0, \quad \int_A \eta^2\, dA = I_\xi = \frac{\pi}{4}(b^4 - a^4), \quad A = \pi(b^2 - a^2). \tag{6.7}$$

The small ovalization of the circular cross section caused by the Poisson-type effects in bending have been ignored; for the analysis of three-dimensional stress state and anticlastic curvature effects in pure bending of nonlinearly elastic prismatic beams with rectangular cross section, see [28]. Thus, after performing the integrations in (6.6), this equation becomes

$$C_1(I_1 - J_1) + C_2(I_2 - J_2) = 0, \tag{6.8}$$

where

$$\begin{aligned} I_1 &= \int_A (1+y\Delta\kappa)^2 dA = \alpha^2 A + I_\xi(\Delta\kappa)^2,\\ I_2 &= \int_A (1+y\Delta\kappa)\,dA = \alpha A, \quad \alpha = 1 + e\Delta\kappa,\\ J_1 &= \int_A \frac{dA}{1+y\Delta\kappa} = \frac{2\pi}{(\Delta\kappa)^2}B_1, \quad B_1 = \sqrt{\alpha^2 - a^2(\Delta\kappa)^2} - \sqrt{\alpha^2 - b^2(\Delta\kappa)^2},\\ J_2 &= \int_A \frac{dA}{(1+y\Delta\kappa)^2} = -\frac{2\pi\alpha}{(\Delta\kappa)^2}B_2, \quad B_2 = \frac{1}{\sqrt{\alpha^2 - a^2(\Delta\kappa)^2}} - \frac{1}{\sqrt{\alpha^2 - b^2(\Delta\kappa)^2}}. \end{aligned} \tag{6.9}$$

For a given $\Delta\kappa$, Eq. (6.9) can be solved numerically for the value of the eccentricity e corresponding to $\Delta\kappa$. The numerical results for the $e = e(\Delta\kappa)$ relationship are shown in Fig. 7a.

We next proceed with the derivation of the moment–curvature relationship. The substitution of (6.4) into the second expression in (6.3) gives

$$M = 2C_1\left[\int_A \eta(1+y\Delta\kappa)^2 dA - \int_A \frac{\eta\, dA}{1+y\Delta\kappa}\right] + 2C_2\left[\int_A \eta(1+y\Delta\kappa)\,dA - \int_A \frac{\eta\, dA}{(1+y\Delta\kappa)^2}\right]. \tag{6.10}$$

Upon performing the integrations, (6.10) can be expressed in the form

$$M = 2C_1(I_3 - J_3) + 2C_2(I_4 - J_4), \tag{6.11}$$

where

$$\begin{aligned} I_3 &= \int_A \eta(1+y\Delta\kappa)^2 dA = 2\alpha I_\xi \Delta\kappa,\\ I_4 &= \int_A \eta(1+y\Delta\kappa)\,dA = I_\xi\Delta\kappa,\\ J_3 &= \int_A \frac{\eta\, dA}{1+y\Delta\kappa} = \frac{A}{\Delta\kappa} - \frac{2\pi\alpha}{(\Delta\kappa)^3}B_1,\\ J_4 &= \int_A \frac{\eta\, dA}{(1+y\Delta\kappa)^2} = \frac{2\pi}{(\Delta\kappa)^3}(B_1 + \alpha^2 B_2). \end{aligned} \tag{6.12}$$

Expression (6.11) is the desired moment–curvature relationship. The corresponding variation $M = M(\Delta\kappa)$ is shown in Fig. 7b. The solid curve corresponds to the nonlinear Mooney–Rivlin model and the dashed line to the linear elastic material model. In the latter case (6.11) reduces to

$$M = EI_\xi\Delta\kappa, \tag{6.13}$$

since the stress $\sigma = \sigma(y)$ is in this case is $\sigma = 6(C_1 + C_2)\epsilon = E\epsilon$, while $e = 0$. For the nonlinear Mooney–Rivlin model, the stress varies nonlinearly along the y direction according to (6.3), which is sketched in Fig. 7c.

6.1. *Straightening of a pre-curved tube*

If a curved tube of initial radius of curvature R_0 is straightened-out by two end couples M, then $R \to \infty$ and $\Delta\kappa = R_0^{-1}$. The corresponding value of M is obtained from (6.11) and (6.11) by replacing $\Delta\kappa$ with $1/R_0$. For example, if $R_0 = 40$ mm, the moment needed to straighten-out the tube is $M = 0.2079$ N m. If the material of the tube was linearly elastic in the entire range of bending, the corresponding moment would have been $M = EI_\xi/R_0 = 0.2243$ N m. In these calculations the inner and outer radii of the tube were assumed to be given by $a = 2.38$ mm and $b = 3.97$ mm, so that $A = 31.72\,\text{mm}^2$ and $I_\xi = 170\,\text{mm}^4$, while $E = 52.8$ MPa.

The normal stress follows from (6.3) by replacing there $\Delta\kappa$ with $1/R_0$, which gives

$$\sigma = 2C_1\left[(1+y/R_0)^2 - \frac{1}{1+y/R_0}\right] + 2C_2\left[(1+y/R_0) - \frac{1}{(1+y/R_0)^2}\right]. \tag{6.14}$$

The magnitudes of the maximum tensile and compressive stresses in this case are

$$\sigma^+_{\max} = 3.47\,\text{MPa}, \quad \sigma^-_{\max} = 6.45\,\text{MPa}, \tag{6.15}$$

corresponding to $y^+ = 4.4$ mm and $y^- = -3.5$ mm, as shown in Fig. 6c.

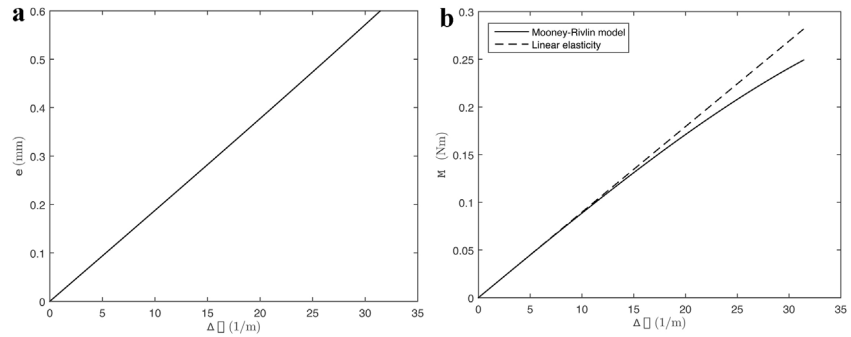

Fig. 7 – (a) The eccentricity e vs. the change in curvature $\Delta\kappa$ in the case of Mooney–Rivlin material model. (b) The applied moment M vs. the change in curvature $\Delta\kappa$ in the case of Mooney–Rivlin material model.

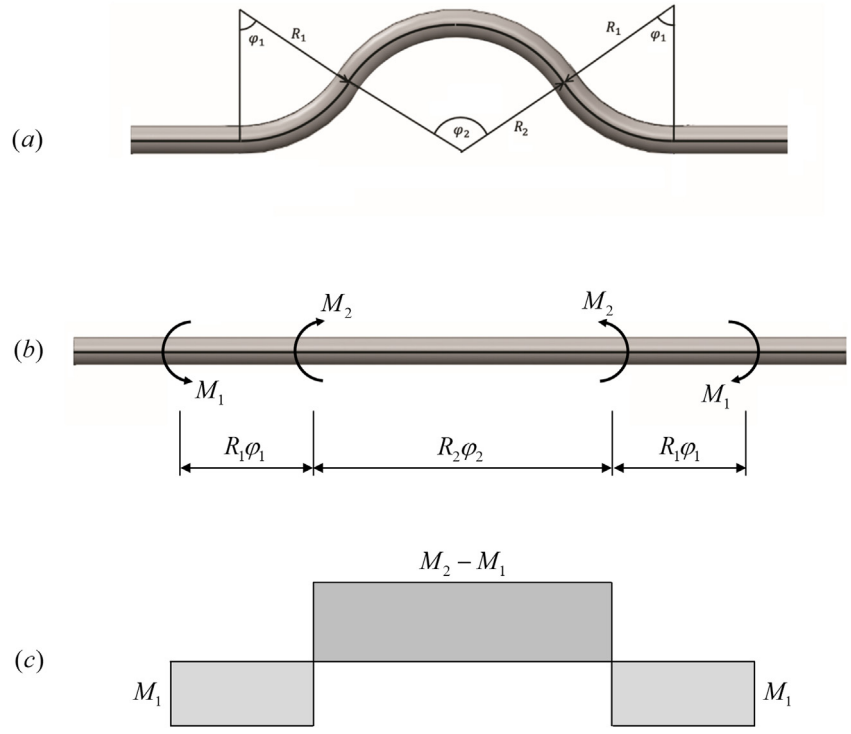

Fig. 8 – (a) The initial pre-curved configuration of the EVA tube. (b) The straightened-out configuration of the tube produced by the application of two pairs of couples M_1 and M_2. (c) The moment diagram along the straightened axis of the tube.

6.2. *Straightening of a doubly pre-curved EVA tube*

Fig. 8b shows a straightened configuration of a doubly pre-curved EVA tube shown in Fig. 8a. Since the pre-curved portions of the tube are circular, the straightening into a perfectly straight configuration can be accomplished by the application of two pairs of concentrated couples of moments M_1 and M_2, because only pure bending by concentrated end couples transforms a circularly pre-curved tube into a straight tube. The magnitude of the moment M_1 is obtained from (6.11) and (6.11) by replacing $\Delta\kappa$ with $1/R_1$, while the magnitude of the moment $M_2 - M_1$ is obtained from (6.11) and (6.11) by replacing $\Delta\kappa$ with $1/R_2$, because the central portion of the tube of radius R_2 is under the bending moment $M_2 - M_1$ (Fig. 8c). For example, if $R_1 = R_2$, the bending moment $M_2 = 2M_1$, regardless of the values of the angles φ_1 and φ_2. The straightened-out configuration of a pre-curved tube is the most critical configuration of the tube, in which the stresses attain their greatest values, because upon the removal of the inserted straight rod, the tube is reverting to its original curved shape, releasing its strain energy and relaxing the stresses caused by the inserted rod. In the case of the cross section of the tube with inner and outer radii $a = 2.38$ mm and $b = 3.97$ mm, the maximum stresses are $\sigma^{+}_{\max} = 3.28$ MPa and $\sigma^{-}_{\max} = 5.65$ MPa in the case of the radii of curvature $R_1 = R_2 = 45$ mm, while $\sigma^{+}_{\max} = 2.59$ MPa and $\sigma^{-}_{\max} = 3.73$ MPa in the case of the radii of curvature $R_1 = R_2 = 65$ mm.

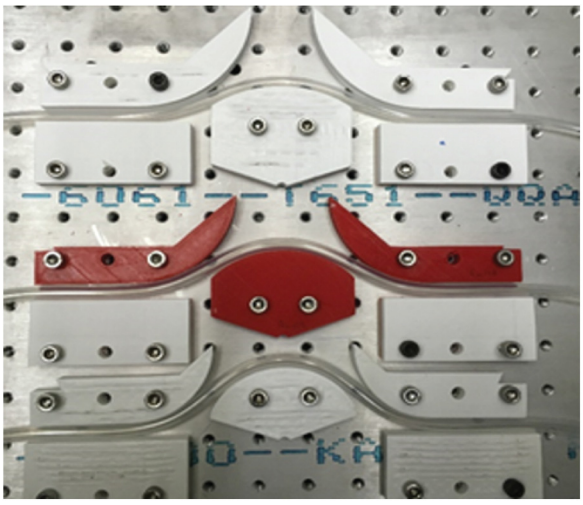

Fig. 9 – Thermoform mold and EVA tubes for different radii of curvature.

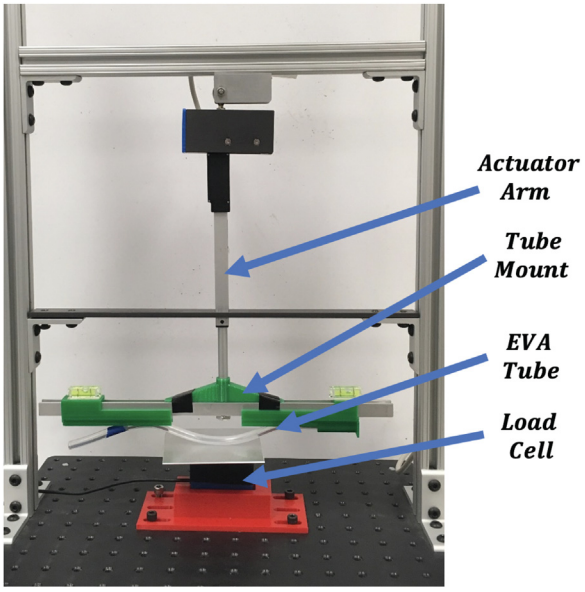

Fig. 10 – Set-up for measurement of force vs. deflection of preformed deflected EVA tubes.

7. Experimental measurement of force vs. deflection of pre-curved EVA tubes

Straight EVA tubes were thermoformed in 3D printed molds (Fig. 9) to attain curved geometry similar to that used in the EDD. The thermoforming process consisted of cutting and fitting the tubes into the mold, heating the mold with the tubes in an oven at 70 °C for 1 h, and, finally, cooling the tubes outside of the oven. The test set-up for measuring the force vs. displacement of pre-curved EVA tubes is shown in Fig. 10. The setup consists of a load cell (SMT 250N), a tube mount, and a vertical actuator arm. One end of the tube is clamped into the mount while the other end of the tube can deflect against a flat surface on the mount. The curved portion of the tube contacts the stationary surface of the load cell. The actuator arm moves the tube mount downward at a speed of approximately 0.1 mm/s and, as the distance decreases between the flat surface on the load cell and the tube mount. The force applied by the deforming tube is measured using the load cell until the tube is straightened.

In Fig. 11a and b, the force vs. displacement is shown for EVA tubes of 7.9 and 9.5 mm outer diameter, respectively, with initial radius of curvature (RoC) of 45, 55, and 65 mm, respectively. From Fig. 11, we observe that the displacement required to generate a particular force increases with decreasing radius of curvature. The tube with a 9.5 mm outer diameter produces a larger force than the tube with 7.5 mm outer diameter keeping all other parameters the same. The tube with a 9.5 mm outer diameter exerts a maximum force of approximately two times that of the tube with a 7.9 mm outer diameter, for all three pre-formed curvatures.

8. Finite element model

To complement and validate the analytical and experimental results shown in the previous sections, a finite element model was developed simulating the straightening of a pre-curved EVA tube. As shown in Fig. 12, the pre-curved and initially stress-free tube is confined between two rigid walls $w1$ and $w2$. The left end of the tube is constrained in all six degrees of freedom, while the right end of the tube is free to move. The surface $w1$ is displaced slowly toward surface $w2$, thereby straightening the tube. The force exerted by the tube on surface $w2$ is determined.

The pre-curved tube geometry was first obtained in 3D (SolidWorks) and meshed using a commercially available finite element program (Hypermesh). Stress and strain as a function of displacement were then obtained using an explicit transient solver (LS-DYNA). All three software packages are commercially available. The mesh for the pre-curved tubes utilized approximately 70,000 8-node quadrilateral elements. Both the linear material model and the nonlinear Mooney–Rivlin model were used, with material parameters determined from the experimental results of Section 7. The initial position of the tube (see Figs. 12 and 13a) corresponds to the case that the insertion rod is completely removed, while the final position of the tube in Fig. 13c corresponds to the case that the (rigid) insertion rod is fully inserted in the EDD. The deformation of a tube being straightened by two rigid walls is physically comparable to the tube being straightened by a rigid inner rod since the cross section inner and outer diameter do not significantly change in either setting. Clearly, our model contains the extreme limiting cases occurring during use of the EDD during surgery. Fig. 13a–c show the von Mises stress along the length of the tube for the initial, intermediate and final position of the rigid wall w1. From Fig. 13, we observe that the von Mises stress varies significantly along the length of the tube. As expected, the largest von Mises stresses occur furthest away from the neutral axis in the y direction.

Fig. 14 shows force vs. displacement and von Mises stress vs. displacement of pre-curved EVA tubes using the Mooney–Rivlin constitutive equations. We observe that the force increases as the displacement increases for all tubes.

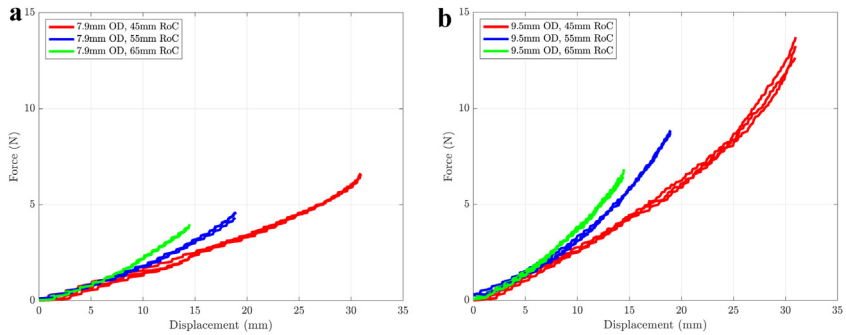

Fig. 11 – Experimentally determined force vs. displacement for: (a) 7.9 mm outer diameter and (b) 9.5 mm outer diameter tube with pre-curved radius of curvature (RoC) of 45, 55, and 65 mm.

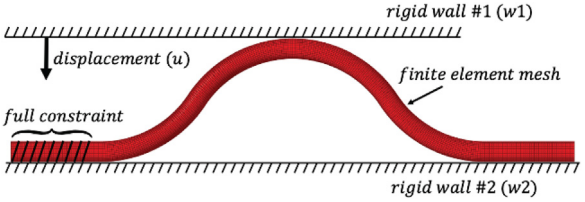

Fig. 12 – Schematic of geometry and boundary conditions.

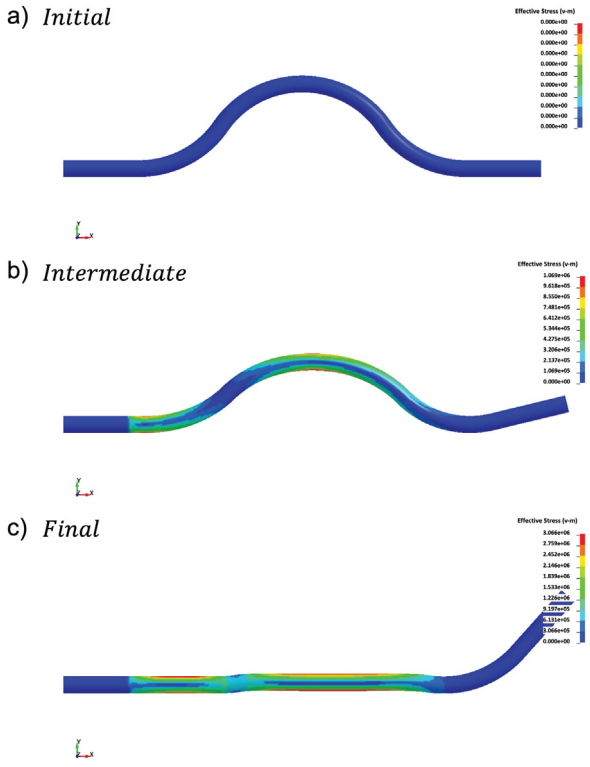

Fig. 13 – The von Mises stress distribution along the length of the tube during its deflection.

We also observe that tubes with a smaller radius of curvature have a larger maximum force. In addition, we observe that the force and the maximum von Mises stress increases as the area moment increases. The maximum von Mises stress varies only a small amount for tubes having different radii of curvature keeping all other parameters constant. On the other hand, tubes with smaller radius of curvature have a larger final value of the von Mises stress, because they deflect a larger total distance compared to the tubes with larger radii of curvature, similar to the trend observed for the simulated force. The numerical results provide insight into the effect of design parameters of the tube on the mechanical performance of the EDD tube. By changing the cross section and the radius of curvature, the force applied against the esophageal wall can vary significantly and, in some cases, the stress can exceed the elastic limit.

In Fig. 15, a comparison is shown for the maximum von Mises stress vs. displacement for the linear and the nonlinear material models. As expected, for small values of displacement there is only a small difference in the calculated values of the force and the maximum von Mises stress for the two models. As the displacement increases, the differences become more pronounced. The linear model overestimates the values of the force and the maximum von Mises stress for a given amount of displacement.

9. Discussion and conclusions

The design parameters of the esophageal deflection device (EDD) strongly influence the performance of the device. The EDD tube exerts forces along the esophageal wall after the insertion rod is removed, thereby deflecting the esophagus. In this paper, the performance of the esophageal deflection device has been studied analytically by evaluating the nonlinear displacements of pre-curved EVA tubes under the action of applied moments. In addition, the displacement of pre-curved EVA tubes has been investigated experimentally using an actuator that applied a known displacement on the tube. Finally, we have simulated the deformation of EVA tubes using finite element analysis. The results from the theoretical, numerical and experimental analysis show that material properties and design parameters such as the radius of curvature of the tube and the cross section of the tube determine the deformation of the tube as well as the internal stresses and strains while the initially curved tube is straightened.

The hyperelastic (Mooney–Rivlin) constitutive model, investigated in Section 5, proved to be of importance in

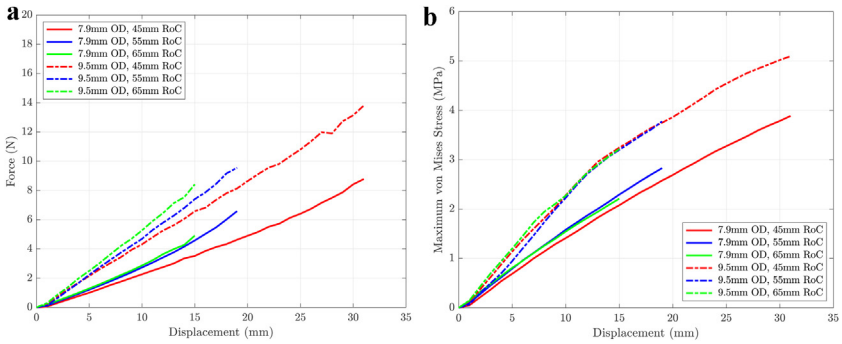

Fig. 14 – The finite element results for the (a) force vs. displacement and (b) maximum von Mises stress vs. displacement using the nonlinear Mooney–Rivlin material model.

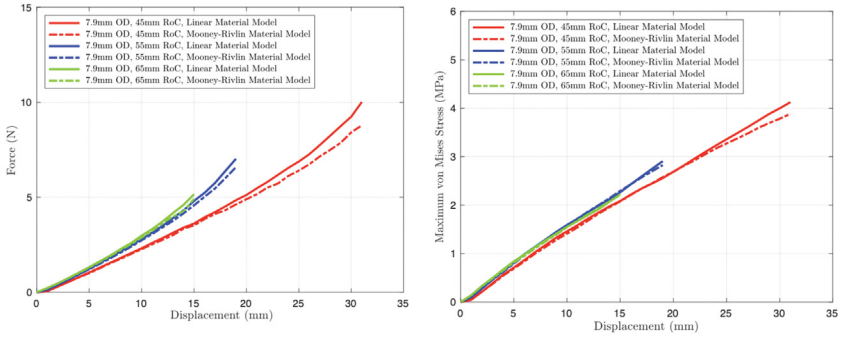

Fig. 15 – Comparison of (a) force vs. displacement and (b) maximum von Mises stress vs. displacement for linear and nonlinear Mooney–Rivlin material models (7.9 mm diameter tubes).

both the analytical and numerical studies. In particular, we observed that an increase in the change of curvature causes the predictions from the linear and nonlinear material models to differ significantly. For the tubes used in this study, the differences became noticeable at an approximate change in curvature of 15 m^{-1}. Additional parameters not studied in this paper may affect the performance characteristics and constitutive equation when the medical device is used clinically. These parameters include viscoelastic (time varying) effects, as well as thermoelastic (temperature dependent) effects. A material with a slower response in releasing its strain energy may make the device easier and safer to use. Thermal effects, with the human body at approximately 37 °C, as opposed to room temperature, can make the device less stiff and, in turn, prevent the device from effectively moving the esophagus. The constitutive equation for the EDD tube material, EVA, needs to be investigated at elevated temperature conditions.

In our analytical evaluation, the curvature remained circular, and the tube cross section remained circular as the tube straightened. The numerical model relaxed those geometrical constraints. Similar results were obtained numerically, but it is clear that the geometric non-linearity observed in the numerical study can affect the stress distribution both along the tube length as well as across the cross section.

In the analytical model, the tube deformation was investigated by changing the curvature due to applied end moments until the tube was straightened. In the experimental and numerical analysis, tube deformation was investigated by moving a rigid surface toward another rigid surface, with the pre-curved tube in-between, in order to straighten the tube. The applied boundary conditions are important for understanding the stress and strain states in the tube and to provide a resulting moment or force, but they do not reveal the effects on the esophageal soft tissue and the body tissue surrounding it. Further experimental and numerical studies should include changing of boundary conditions to address worst-case scenarios and extreme anatomical conditions. With the aim of moving the esophagus safely and reliably, it would be desirable to enhance the model and investigate the interactions of the tube with the soft tissue. Future *ex vivo* studies (e.g., using a porcine model) could provide useful results for this application. In all investigations, the consideration of how design changes affect patient safety must be of primary concern.

In summary, the conclusions of our study are as follows.

- The EDD has been designed and manufactured to exert a force on the esophagus and deflect it away from the ablation site during surgery.
- Previous EDD-like devices have required expensive and complicated manufacturing methods [4–6]. A low cost EVA tube thermoforming process has been implemented to vary the dimensions of the EDD tube curvature and cross section.
- The previously known mechanical properties for the EVA tube material, shown in Table 1, were inadequate for modeling the constitutive response during deformation of the

EDD due to the large deformation states that are beyond the linear elastic range (>1%).

- Uniaxial tensile tests were performed on the specific EVA formulation provided by the supplier and after thermoforming. We observe that the EVA tube material is hyperelastic with estimated Mooney–Rivlin parameters $C_1 = -27.4$ MPa and $C_2 = 36.2$ MPa. In the range of infinitesimal strain, EVA can be modeled as a linearly elastic material with a modulus of elasticity $E = 52.8$ MPa.
- Moment–curvature and stress–curvature relationships were determined analytically using both linear and nonlinear constitutive equation. The analytical approach reveals direct relationship between design features and product performance including the effect of curvature, cross section, and radial location on applied moment and stresses. Maximum stress values for one proposed design in a straightened state were found to be $\sigma^{+}_{max} = 3.28$ MPa and $\sigma^{-}_{max} = 5.65$ MPa, respectively, indicating potential plastic deformation.
- Experimental measurements of the force exerted by the tube during straightening range from 0 to 14 N. The force was shown to depend on the deformation state during straightening as well as the initial radius of curvature and cross section of the tube.
- A numerical model, incorporating linear and nonlinear material models, was developed using finite element analysis to simulate the deformation of pre-curved tubes and determine the stress strain behavior of the pre-curved tubes in the EDD. This model can be extended to evaluate different geometries, materials, or boundary conditions.
- The analytical and numerical model revealed levels of von Mises stress beyond the elastic limit. Those limits should be avoided when finalizing the EDD design to prevent plastic deformation.
- Significant differences between the tube deformation predictions based on linear and nonlinear material models occurred at a large change in curvature ($>15\ m^{-1}$) for both the analytical and numerical studies. A non-linear material model is necessary to accurately model the expected deformation of the EDD.
- Further studies should be undertaken to investigate the performance of the device during *ex vivo* and *in vivo* testing, including a more detailed and accurate description of the interactions of the device with surrounding soft tissue at body temperature. Patient safety is of upmost importance when translating this device for clinical use.

Conflicts of interest

None declared.

Acknowledgments

We are grateful for insightful discussions with Dr. Thomas Savides, MD and Dr. Gregory Feld, MD from UCSD's School of Medicine. We acknowledge support for this study from Circa Scientific (Lee Geist) and from UCSD's ACTRI Galvanizing Engineering and Medicine Program. Steve Porter, Jessica Tuazon, Weilun Hsieh, Matthew Kohanfars, and Tanvir Reza helped with setting up the experiments; we are grateful for their help.

REFERENCES

[1] Chugh SS, Havmoeller R, Narayanan K, Singh D, Rienstra M, Benjamin EJ, et al. Worldwide epidemiology of atrial fibrillation: a global burden of disease 2010 study. Circulation 2013;129(8):837–47, http://dx.doi.org/10.1161/CIRCULATIONAHA.113.005119.

[2] Spragg D, Calkins H. Catheter ablation for atrial fibrillation: past, present, and future. In: Steinberg JS, Jaïs P, Calkins H, editors. Practical guide to catheter ablation of atrial fibrillation. Hoboken: John Riley & Sons; 2015. p. 7–15, http://dx.doi.org/10.1002/9781118658369.ch02.

[3] Kaneshiro T, Matsumoto Y, Hijioka N, Nodera M, Yamada S, Kamioka M, et al. Distinct forms of esophageal lesions after radiofrequency and cryoballoon pulmonary vein isolation. JACC: Clin Electrophysiol 2018;4(12):1642–3, http://dx.doi.org/10.1016/j.jacep.2018.08.006.

[4] Elkhatib I, Syed F, Krinsky ML, Savides TJ, Feld G. Endoscopic mechanical displacement of the esophagus during atrial fibrillation catheter ablation. Gastrointest Endosc 2014;79(5):AB511–12, http://dx.doi.org/10.1016/j.gie.2014.02.806.

[5] Koruth JS, Reddy VY, Miller MA, Patel KK, Coffey JO, Fischer A, et al. Mechanical esophageal displacement during catheter ablation for atrial fibrillation. J Cardiovasc Electrophysiol 2012;23(2):147–54, http://dx.doi.org/10.1111/j. 1540-8167.2011.02162.x.

[6] Parikh V, Swarup V, Hantla J, Vuddanda V, Dar T, Yarlagadda B, et al. Feasibility, safety, and efficacy of a novel preshaped nitinol esophageal deviator to successfully deflect the esophagus and ablate left atrium without esophageal temperature rise during atrial fibrillation ablation: the DEFLECT GUT study. Heart Rhythm 2018;15(9):1321–7, http://dx.doi.org/10.1016/j.hrthm.2018.04.017.

[7] Morris K, Savides T, Feld G, Seo Y, Fu Y, Talke FE, Esophageal deflection device. US 2020/0029822 (2020). Published Patent (Pending).

[8] Garner S, Morris K, Pegan R, Savides TJ, Talke FE. Development of a luminal esophageal temperature monitoring device for use during treatment for atrial fibrillation. In: American Society for Mechanical Engineers, editor. Proceedings of the ASME-JSME 2018 joint international conference on information storage and processing systems and micromechatronics for information and precision equipment. 2018. p. 1–3, http://dx.doi.org/10.1115/ISPS-MIPE2018-8578.

[9] Garner S. Development of a luminal esophageal temperature monitoring device for use during treatment of atrial fibrillation [M.Sc. dissertation]. La Jolla, San Diego: University of California; 2018.

[10] Morimoto TK, Greer JD, Hawkes EW, Hsieh MH, Okamura AM. toward the design of personalized continuum surgical robots. Ann Biomed Eng 2018;46:1522–33, http://dx.doi.org/10.1007/s10439-018-2062-2.

[11] Webster RJ, Okamura AM, Cowan NJ. Toward active cannulas: miniature snake-like surgical robots. In: Institute of Electrical and Electronics Engineers, editor. Proceedings of the IEEE/RSJ international conference on intelligent robots and systems. 2006. p. 2857–63, http://dx.doi.org/10.1109/IROS.2006.282073.

[12] Rucker DC, Jones BA, Webster RJ. A geometrically exact model for externally loaded concentric-tube continuum robots. IEEE Trans Robot 2010;26(5):769–80, http://dx.doi.org/10.1109/TRO.2010.2062570.

[13] Antman SS. Nonlinear problems of elasticity. 2nd ed. New York: Springer; 2005, http://dx.doi.org/10.1007/0-387-27649-1.
[14] Baek C, Yoon K, Kim D. Finite element modeling of concentric tube continuum robots. Struct Eng Mech 2016;57(5):809–21, http://dx.doi.org/10.12989/sem.2016.57.5.809.
[15] Morimoto TK, Okamura AM. Design of 3-D printed concentric tube robots. IEEE Trans Robot 2016;32(6):1419–30, http://dx.doi.org/10.1109/TRO.2016.2602368.
[16] Biase LD, Saenz LC, Burkhardt DJ, Vacca M, Elayi CS, Barrett CD, et al. Esophageal capsule endoscopy after radio frequency catheter ablation for atrial fibrillation: documented higher risk of luminal esophageal damage with general anesthesia as compared with conscious sedation. Circ: Arrhyth Electrophysiol 2009;2(2):108–12, http://dx.doi.org/10.1161/CIRCEP.108.815266.
[17] Zhang P, Zhang Y-Y, Ye Q, Jiang R-H, Liu Q, Ye Y, et al. Characteristics of atrial fibrillation patients suffering esophageal injury caused by ablation for atrial fibrillation. Sci Rep 2020;10:2751, http://dx.doi.org/10.1038/s41598-020-59539-6.
[18] Berjano EJ, Hornero F. What affects esophageal injury during radiofrequency ablation of the left atrium? An engineering study based on finite-element analysis. Physiol Meas 2005;26(5):837–48, http://dx.doi.org/10.1088/0967-3334/26/5/020.
[19] Liao D, Frøkjær JB, Yang J, Zhao J, Drewes AM, Gilja OH, et al. Three-dimensional surface model analysis in the gastrointestinal tract. World J Gastroenterol 2006;12(19):2870–5, http://dx.doi.org/10.3748/wjg.v12.i18.2870.
[20] Jernigan SR, Buckner GD, Eischen JW, Cormier DR. finite element modeling of the left atrium to facilitate the design of an endoscopic atrial retractor. J Biomech Eng 2007;129(6):825–37, https://doi.org/10.1115/1.2801650.
[21] Hirdes MM, Vleggaar FP, de Beule M, Siersema PD. In vitro evaluation of the radial and axial force of self-expanding esophageal stents. Endoscopy 2013;45:997–1004, http://dx.doi.org/10.1055/s-0033-1344985.
[22] Evonavich RF III, Nori DM, Haines DE. A randomized trial comparing effects of radiofrequency and cryoablation on the structural integrity of esophageal tissue. J Interv Cardiac Electrophysiol 2007;19:77–83, http://dx.doi.org/10.1007/s10840-007-9142-9.
[23] Natali AN, Carniel EL, Gregersen H. Biomechanical Behaviour of Oesophageal tissues: material and structural configuration. Experimental data and constitutive analysis. Med Eng Phys 2009;31(9):1056–62, http://dx.doi.org/10.1016/j.medengphy.2009.07.003.
[24] US Food and Drug Administration. Use of international standard ISO 10993-1; 2020 https://www.fda.gov/downloads/medicaldevices/deviceregulationandguidance/guidancedocuments/ucm348890 [accessed 25 March 2020].
[25] Ogden RW. Nonlinear elasticity, anisotropy, material stability and residual stresses in soft tissue. In: Holzapfel GA, Ogden RW, editors. Biomechanics of soft tissue in cardiovascular systems. Vienna: Springer; 2003. p. 65–108, http://dx.doi.org/10.1007/978-3-7091-2736-03.
[26] Lubarda VA. Elastoplasticity theory. Boca Raton: CRC Press; 2001.
[27] Morris KM, Rosenkranz A, Seibert H, Ringel L, Diebels S, Talke FE. Uniaxial and biaxial testing of 3D printed hyperelastic photopolymers. J. Appl. Polym. Sci 2019:48400, http://dx.doi.org/10.1002/app.48400.
[28] Lanzoni L, Tarantino AM. Finite anticlastic bending of hyperelastic solids and beams. J Elast 2018;131:137–70, http://dx.doi.org/10.1007/s10659-017-9649-y.